Spatial distribution of defect luminescence in ZnO nanorods: an investigation by spectral cathodoluminescence imaging

Liangchen Zhu, Mark Lockrey, Matthew R. Phillips, and Cuong Ton-That*

Dr. L. Zhu, Dr. M. Lockrey, Prof. M. R. Phillips, and Assoc. Prof. C. Ton-That

School of Mathematical and Physical Sciences, University of Technology Sydney, Ultimo, NSW 2007, Australia

E-mail: cuong.ton-that@uts.edu.au

Abstract

The spatial distribution of ubiquitous green luminescence (GL) in ZnO nanorods is investigated using cathodoluminescence (CL) spectral imaging. The vertically aligned, single-crystal nanorods exhibit a strong GL emission at 2.42 eV at 80 K, attributable to oxygen vacancies. The spectral imaging reveals the GL emission is predominantly located in the surface layer of nanorods; the thickness and intensity of this layer decreases rapidly at elevated temperatures. On the other hand, the near-band-edge emission is weakest near the nanorod edges. The temperature-dependent CL maps are consistent with the properties of a model in which singly ionized oxygen vacancies are stabilized by the surface band bending, which leads to the GL enhancement at the expense of near-band-edge emission. These results demonstrate the utility of spectral CL imaging to map the spatial distribution of defect luminescence in nanostructured materials.

1. Introduction

ZnO is a multifunctional wide bandgap semiconductor, which has been exploited in various areas including nanomedicine, optoelectronics, and catalysis.[1,2] It is well known that ZnO nanostructures, such as nanowires and nanosheets, can contain a high density of points defects, especially zinc (V_{Zn}) and oxygen vacancies (V_O).[3,4] Understanding the role of defects and their spatial distribution in nanostructures, especially defects at interfaces, is important since they can strongly affect the electrical properties and performance of ZnO-based nanodevices.[5,6] It is generally accepted that V_O is responsible for green luminescence (GL) at ≈ 2.4 eV in ZnO grown under oxygen-deficient conditions; however, the exact chemical origin of this emission remains controversial and has been attributed to V_O defects in either neutral[7,8] or singly charged state.[9,10] Despite the abundant research on the GL emission in ZnO, the spatial distribution of this emission in nanostructures and its temperature dependencies have been scarcely investigated.

While confocal Raman and photoluminescence microscopy is capable of measuring individual sub-micron structures, the spatial resolution and the accuracy of the techniques are limited by poor signal to noise ratio and the diffraction limit.[7,11,12] In comparison, cathodoluminescence (CL) spectral imaging, which utilizes highly focused electron beam with a spot size of a few nanometers, allows nanocharacterization of individual nanostructures, which themselves might have non-uniform local properties. In this paper, an example of the application of CL spectral imaging to ZnO nanorods is provided to investigate the characteristics of the GL and its spatial distribution within individual ZnO nanostructures. The spectral imaging technique reveals a profound radial variation of GL intensities within individual nanorods. The spatial distribution of GL centers is found to be highly sensitive to an

increase in temperature, which accounts for often contradictory interpretations of the role of native defects in nanostructures in the open literature.

2. Experimental Section

Highly ordered ZnO nanorods were grown onto an *a*-plane sapphire via the chemical vapor transport method using Au nanoparticles as catalyst, as described in detail elsewhere.[13] Briefly, a ZnO:graphite powder mixture with 1:1 weight ratio was heated at 900°C as source material under a constant flow of Ar gas at ≈100 mbar pressure. The *a*-plane sapphire substrate was pre-deposited with a 3 nm thick layer of Au, which acts as a catalyst for nanorod growth. X-ray diffraction (not shown) confirms the nanorods are vertically aligned along the ZnO *c*-axis. Spectral CL images were acquired using a FEI Quanta 200 scanning electron microscope (SEM) equipped with a custom-built hyperspectral imaging and spectrometry system, which consists of a parabolic mirror, an optical fibre, an Oriel MS257 monochromator and a Hamamatsu S7011-1007 CCD sensor, which consists of 1044×124 active pixels. The schematic overview of the experimental setup is presented in Figure 1(a), showing its hot and cold stages. As the electron beam scans across a sample, an entire CL spectrum is recorded per pixel building up a 3D hyperspectral data set. A typical CL hyperspectral set consists of 512×512 pixels with each pixel containing a full CL spectrum over the wavelength range from 200 to 900 nm (Figure 1b). In this work at an accelerating voltage of 10 kV, the radial energy loss distribution can be simulated using the CASINO Monte Carlo simulation code[14] and reveals that 70% of the energy loss occurs within a radius of ≈60 nm. The diffusion length of minority carriers in ZnO nanorods is ≈240 nm.[15] Combining these terms gives an effective CL spatial resolution of ≈250 nm at 10 kV accelerating voltage. To analyze the spatial variation of a particular emission, an intensity map can be generated by selecting a region-of-interest (ROI) energy window; in this work the windows were set around the GL peak energy at 2.46 eV and

the near-band-edge (NBE) energy at 3.32 eV. All CL spectral data were corrected for the overall wavelength-dependent detection sensitivity of the system.

3. Results and discussion

The top view SEM image of the ZnO nanorods, displayed in Figure 2(a), shows a highly ordered array of single-crystal ZnO nanorods. The nanorods possess hexagonal symmetry and are perpendicular to the *a*-sapphire substrate, indicating epitaxial growth on the lattice-matched *a*-sapphire substrate with the nanorod sidewalls being the {1-100} ZnO facets. The ZnO nanorods are ≈4 μm long with diameters in the range of 0.4 – 1.2 μm. Figure 2(b,c) shows the corresponding CL images, which map the spatial distributions of the near-band-edge (NBE) and GL intensities, respectively. Since the NBE and GL ROI maps were extracted from the same hyperspectral scan with minimized external perturbations, this allows direct correlation with the morphology of the nanorod array. While individual nanorods exhibit similar luminescence properties with a sharp NBE peak at 3.27 eV and a broad GL band centered at 2.42 eV at 300 K [Figure 2(d)], the spatial distributions of these emissions vary strongly across the cross section of a nanorod. The NBE emission is strongest in the interior of the ZnO nanorods and virtually absent in the near-edge surface regions. In contrast, the GL is mostly concentrated in the near-edge layer of a thickness of ≈200 nm at room temperature. A comparison with literature suggests that the GL at 2.46 eV is likely caused by the radiative recombination of a hole with an electron at V_O.[4,9] Previous work by our groups and others on the annealing of ZnO in Zn-rich and O-rich conditions revealed that the green bands at ≈2.3 and ≈2.5 eV at 80 K can be attributed to the V_{Zn}-related defects and V_O centers, respectively.[4,16,17] Since the (0001) top surface of most nanorods is flat, these spatial variations in the NBE and GL intensities are likely caused by a high density of radiative V_O defects in the near-surface region of ZnO nanocrystals. Similar observations of near-surface GL enhancement have been reported previously.[7,18] The GL in the core of the nanorods has an identical emission

peak position and FWHM as the GL at the surface (Figure 2[d]). Based on these spectral similarities, we suggest that the core GL emission is resulted from wave guiding effects as the near-edge GL emission is guided by the nanorod to the top surface.

For CL spectral imaging, effects of scattered primary electrons by nanostructures must be considered in order to correctly interpret luminescence images. While all the nanorods were resolved clearly as individual emitters by the CL imaging technique, imaging artefacts can arise if forward-scattered electrons generate CL in surrounding nanorods as shown in the simulated trajectories of 10^5 incident electrons in two adjacent nanorods in Figure 3(a). This is due to the fact that the CL parabolic mirror collects all emitted light from a sample area of ≈30 μm diameter. The effect of electron forward and back scattering can be very significant in spectral imaging since nanostructured materials are typically decorated with luminescent surface defects. In order to prove there are no significant artefacts in the spectral images in Figure 2, we simulated electron energy loss profiles in two adjacent ZnO nanorods that have similar dimensions (nanorod diameter 0.5 μm and separation 0.3 μm) to those in Figure 2(a) using the Monte Carlo simulation CASINO.[14] Our previous work showed that the electron energy loss contours within the electron interaction volume can accurately predict the in-plane and in-depth CL spatial distribution in a solid specimen.[19] As shown in Figure 3(b), the energy loss profiles at 10 kV are slightly shifted towards the center between the two nanorods; this shift is due to CL excitation caused by forward-scattered electrons from the other nanorod. The very slight concentric variation of the loss profiles with respect to the hexagonal nanorod shape indicates that these profiles are not significantly affected by the presence of the other nanorod in its vicinity. This is illustrated more clearly in the lateral profile of the energy loss across the two nanorods in Figure 3(b). Even when the excitation point is near the edge of a nanorod, the CL contribution from surrounding nanorods is negligibly small. Combination of the simulation results and the spectral CL maps suggests that the difference in the local luminescence

properties of the near-surface and core regions within individual nanowires is due to the presence of luminescent V_O defects in an axial surface layer. This finding is consistent with oxygen-deficient growth conditions for the nanorods used in this work.

To gain further insight into the properties of V_O defects in the near-surface region, the spatial dependence of the emissions was further investigated by acquiring CL maps of the GL at elevated temperatures up to 423 K (Figure 4). It can be seen in these maps that the intensity and width of the GL surface layer decreases quickly with increasing temperature and totally disappears at 423 K. There is a weak GL emission from the core of the ZnO nanorods which appears to become stronger relative to the surface GL as both quench with increasing temperature. The emission from the core is likely due to wave guiding effects as the GL from the near-edge is out-coupled with the nanorod. The luminescence behavior of the near-edge GL is displayed more clearly in the line profiles of the GL across a nanorod edge in Figures 5(b), which shows the rapid thermal quenching of the GL near-surface layer relative to the background emission in the interior of the nanorods at elevated temperatures. Concurrently the GL layer becomes thinner and moves further out to the nanorod edge. Curve fitting of the GL line profile was made with a Gaussian peak fitted to the right half of the profile, yielding the full width at half maximum (FWHM) of the GL spatial layer as a function of temperature. As temperature is increased from room temperature to 423 K, the GL layer width decreases considerably from 162 ± 22 nm to 72 ± 6 nm as presented in Figure 5(b). The GL peak is red shifted with increasing temperature, which can be explained by the reduction in the ZnO band gap due to the electron-phonon effect. The energy shift of the GL peak (≈ 0.021 eV) over the temperature range is smaller than that of the NBE emission (0.071 eV). The deep level associated with V_O defects is not expected to shift in proportion to the shift of the band edges since the thermal population of the defects also affects the transition energy. At elevated temperatures the GL emission from the core of ZnO nanorods becomes relatively stronger

compared with the near-edge GL, probably due to the desorption of adsorbed oxygen species from the ZnO surface (discussed further below).

A possible model that explains the observed temperature-dependent spectral maps is that singly ionized V_O^+ is stabilized by the band bending at the ZnO surface as shown in the model in Figure 6. It is generally accepted that oxygen adsorption (which can occur at room temperature under ambient conditions) on the ZnO surface can cause an upward band bending by capturing electrons in the near-surface region,[20] because chemisorbed oxygen behaves as an electron acceptor on the ZnO surface.[21] The pinned Fermi level of the nanorods, expected to be close to the conduction band edge due to n-type auto-doping during growth, should stay above the $V_O^{0/2+}$ charge transfer level in the flat band region thus the interior of nanorods is populated with V_O^0. In the near-surface region, with a sufficient degree of upward band bending V_O should be in the V_O^{2+} charge state, producing a surface depletion layer.[22] It is worth noting that this depletion layer is much narrower than the radius of the nanorods used in this study.

Theoretical calculations predicted that V_O^+ is higher in energy than both V_O^0 and V_O^{2+} and behaves as a negative-U center under equilibrium conditions;[23,24] however, V_O^+ could exist in the near-surface region since V_O^{2+} can temporarily capture an electron from a trap state,[10] which is likely associated with surface states. Consequently, V_O^+ states in the surface region of ZnO nanorods can be stabilized by the formation of the electron depletion layer. Due to the upward band bending, the $V_O^{0/2+}$ charge transfer level deflects above the Fermi level converting V_O^0 to V_O^{2+}, which then in turn captures an electron from surface states to produce singly ionized V_O^+, which behaves as the initial state of the GL emission.[7,22] Holes are swept into the depletion region and recombine with electrons at V_O^+, resulting in a highly efficient GL channel. This model is consistent with the rapid quenching of the GL surface emission (see Figure 5[a]) at elevated temperatures, due to desorption of adsorbed oxygen species. With the rise of

temperature, the desorption of adsorbed oxygen species from the ZnO surface and the thermalization of the related surface states are enhanced,[25-27] thus reducing the surface band bending and the width of the electron depletion layer. The decrease of the depletion layer width and band flattening lead to a portion of near-surface V_O^{2+} states reverting into V_O^0, which accounts for the rapid thermal quenching of the near-edge GL shown in Figure 5. Accordingly the near-surface GL emission region becomes thinner and is pushed further out toward the surface with increasing temperature. In this depletion region the NBE is strongly suppressed. When the surface field is sufficiently strong, electrons and holes are swept in opposite directions, leading to the disassociation of e-h pairs. Additionally, the NBE is also quenched by competitive recombination at V_O^+ centers in the band bending region.

4. Conclusion

In summary, we demonstrated that spectral CL imaging can provide useful information on radiative defects in semiconductor nanostructures, which is not accessible by other luminescence spectroscopy techniques. The results from the imaging of the ZnO nanorod cross-sections reveal that the axial near-surface green emission arises from surface band bending converting V_O^0 to V_O^{2+}, which becomes surface located V_O^+ centers via electron capture from surface states. The rapid reduction in the green emission area in the nanorods with increasing temperature occurs likely because of thermally stimulated desorption of adsorbed oxygen species, which flattens the surface bands returning the near-surface oxygen vacancies to their neural state. Accordingly, luminescence inhomogeneity and its temperature dependencies need to be considered in order to correctly explain defect luminescence in ZnO and other semiconductor nanostructures.

References

[1] J. Wang, J. S. Lee, D. Kirn, L. Zhu, *Acs Appl. Mater. Interfaces* **2017**, *9*, 39971.

[2] A. B. Djurisic, A. M. C. Ng, X. Y. Chen, *Prog. Quantum Electron.* **2010**, *34*, 191.

[3] K. Seo, M. Suh, S. Ju, *Electron. Mater. Lett.* **2013**, *9*, 273.

[4] C. Ton-That, L. Weston, M. R. Phillips, *Phys. Rev. B* **2012**, *86*, 115205.

[5] C.-Y. Chen, J. R. D. Retamal, I. W. Wu, D.-H. Lien, M.-W. Chen, Y. Ding, Y.-L. Chueh, C.-I. Wu, J.-H. He, *ACS Nano* **2012**, *6*, 9366.

[6] K. M. Wong, Y. G. Fang, A. Devaux, L. Y. Wen, J. Huang, L. De Cola, Y. Lei, *Nanoscale* **2011**, *3*, 4830.

[7] K. M. Wong, S. M. Alay-e-Abbas, Y. Fang, A. Shaukat, Y. Lei, *J. Appl. Phys.* **2013**, *114*, 034901.

[8] Y. Hu, H. J. Chen, *J. Appl. Phys.* **2007**, *101*, 124902.

[9] K. Vanheusden, W. L. Warren, C. H. Seager, D. R. Tallant, J. A. Voigt, B. E. Gnade, *J. Appl. Phys.* **1996**, *79*, 7983.

[10] P. Camarda, F. Messina, L. Vaccaro, S. Agnello, G. Buscarino, R. Schneider, R. Popescu, D. Gerthsen, R. Lorenzi, F. M. Gelardi, M. Cannas, *Phys. Chem. Chem. Phys.* **2016**, *18*, 16237.

[11] A. C. Gandhi, H.-J. Hung, P.-H. Shih, C.-L. Cheng, Y.-R. Ma, S. Wu, *Nanoscale Res. Lett.* **2010**, *5*, 581.

[12] Z. Y. Fan, P. C. Chang, J. G. Lu, E. C. Walter, R. M. Penner, C. H. Lin, H. P. Lee, *Appl. Phys. Lett.* **2004**, *85*, 6128.

[13] C. Ton-That, M. Foley, M. R. Phillips, *Nanotechnology* **2008**, *19*, 415606.

[14] D. Drouin, A. R. Couture, D. Joly, X. Tastet, V. Aimez, R. Gauvin, *Scanning* **2007**, *29*, 92.

[15] A. Soudi, P. Dhakal, Y. Gu, *Appl. Phys. Lett.* **2010**, *96*, 253115.

[16] J. Čížek, J. Valenta, P. Hruška, O. Melikhova, I. Procházka, M. Novotný, J. Bulíř, *Appl. Phys. Lett.* **2015**, *106*, 251902.

[17] C. Ton-That, M. R. Phillips, M. Foley, S. J. Moody, A. P. J. Stampfl, *Appl. Phys. Lett.* **2008**, *92*, 261916.

[18] M. Foley, C. Ton-That, M. R. Phillips, *Appl. Phys. Lett.* **2008**, *93*, 243104.

[19] M. Toth, M. R. Phillips, *Scanning* **1998**, *20*, 425.

[20] B. F. Spencer, D. M. Graham, S. J. O. Hardman, E. A. Seddon, M. J. Cliffe, K. L. Syres, A. G. Thomas, S. K. Stubbs, F. Sirotti, M. G. Silly, P. F. Kirkham, A. R. Kumarasinghe, G. J. Hirst, A. J. Moss, S. F. Hill, D. A. Shaw, S. Chattopadhyay, W. R. Flavell, *Phys. Rev. B* **2013**, *88*, 195301.

[21] M. Oku, *Jpn. J. Appl. Phys. Part 1-Regul. Papers Short Notes Rev. Papers* **1993**, *32*, 4377.

[22] D. Wang, N. Reynolds, *ISRN Condens. Matter Phys.* **2012**, *1*, 950354.

[23] C. G. Van de Walle, *Phys. B-Condens. Matter* **2001**, *308*, 899.

[24] A. Janotti, C. G. Van de Walle, *Appl. Phys. Lett.* **2005**, *87*, 3.

[25] W. Hideo, W. Masanobu, T. Tadashi, *Jpn. J. Appl. Phys.* **1965**, *4*, 945.

[26] M. Zhu, H. Huang, J. Gong, C. Sun, *J. Appl. Phys.* **2007**, *102*, 043106.

[27] D. Wang, H. W. Seo, C. C. Tin, M. J. Bozack, J. R. Williams, M. Park, N. Sathitsuksanoh, A.-j. Cheng, Y. H. Tzeng, *J. Appl. Phys.* **2006**, *99*, 113509.
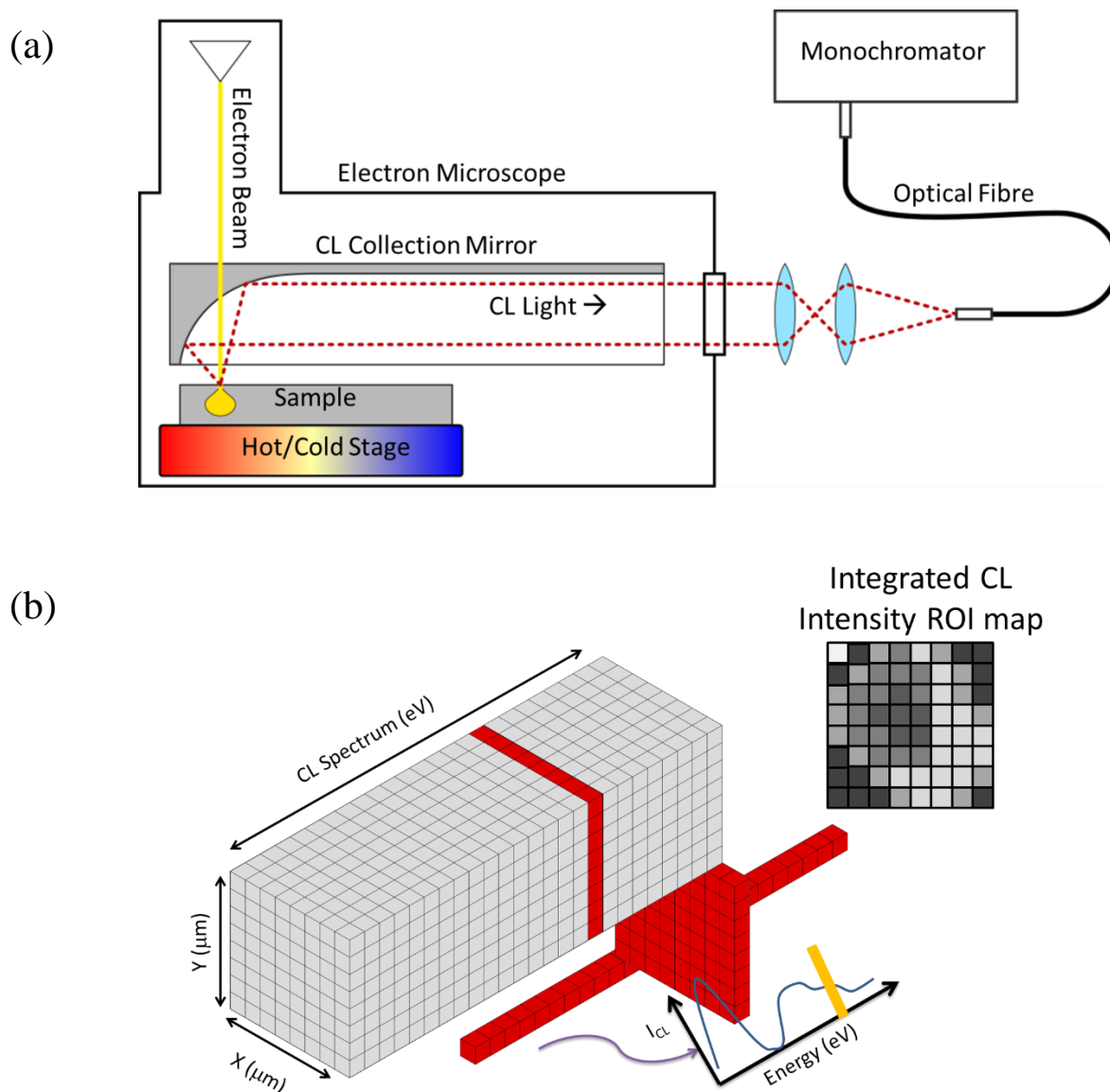
Figure 1. (a) Schematic showing the hyperspectral CL imaging system which consists of collection optics introduced into an SEM. Light emitted from the sample is collected by parabolic mirror and analysed by an Oriel MS257 monochromator and a CCD sensor. (b) As the electron beam scans across a sample, an entire CL spectrum is recorded per pixel building up a 3D hyperspectral data set. An intensity map can be generated from the 3D data set by selecting a region-of-interest (ROI) energy window to display the spatial variation in the integrated intensity of a particular emission.

Figure 2. (a-c) SEM image of the ZnO nanorods and corresponding CL ROI maps at 80 K for NBE and GL emission for 3.32 and 2.46 eV, respectively (E_B = 10 keV and I_B = 0.75 nA). Comparison of the CL maps reveals a strong spatial anti-correlation between NBE and GL emissions. The bright margins in the GL ROI map indicate the GL mostly originates from the near-surface layer of the nanorods. (d) Comparison of the CL spectra recorded in the core and near-edge regions of a ZnO nanorod at 300 K. Inset: schematic illustration of spatial distributions of NBE and GL emissions over the nanorod top surface.
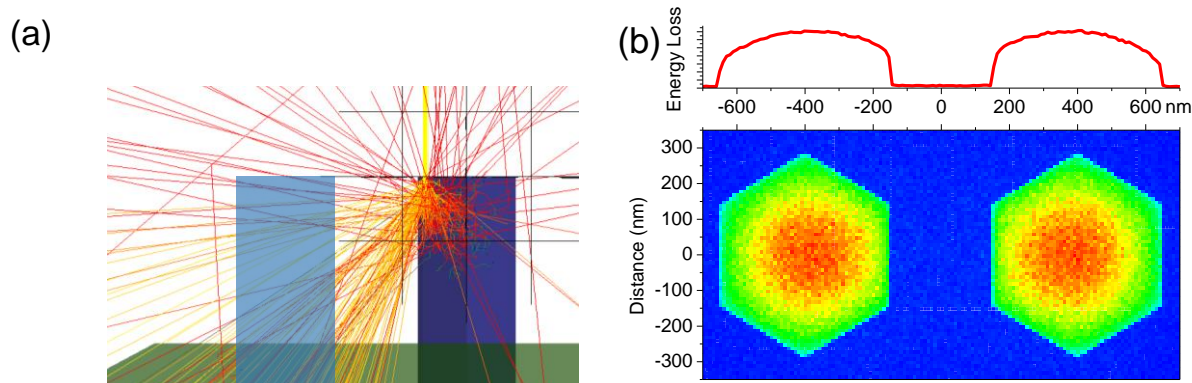
(a)

(b)

Figure 3. (a) CASINO Monte Carlo simulation of electron trajectory in adjacent ZnO nanorods. Imaging artifacts can arise if forward scattered electrons from a nanorod excites CL in surrounding nanorods since the CL collection mirror collects all light from a sample area of ≈30 µm diameter. (b) Simulated electron energy loss profiles at 10 kV for two adjacent nanorods with dimensions and spacing similar to those in Figure 2 (nanorod diameter = 0.5 µm, separation = 0.3 µm), showing the loss profiles are almost concentric with the hexagonal nanorods. This indicates the CL intensity maps are not significantly affected by electron scattering in adjacent nanorods.
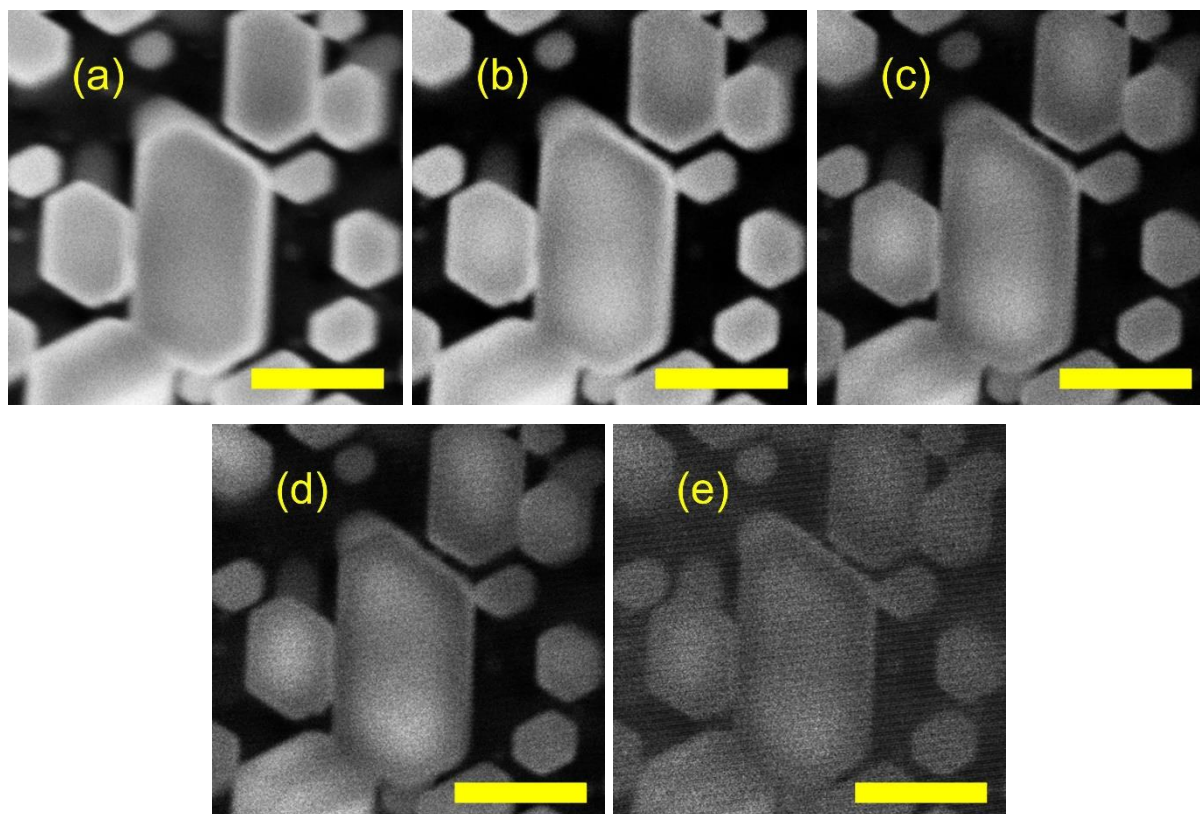
Figure 4. CL maps of the GL acquired at elevated temperatures: (a) 303 K, (b) 328 K, (c) 358 K, (d) 373 K and (e) 423 K (e). CL acquisition conditions: $V_B = 10$ kV, $I_B = 0.75$ nA. All the scale bars are 1 μm. The CL intensity of the near-surface GL margins decreases rapidly with increasing temperature and merge into the background emission in the nanorod core at 423 K. This luminescence behavior is consistent with the flattening of the bands at high temperatures. The weak GL emission from the nanorod cores could be due to wave guiding effects as the GL from the side wall is out-coupled with the nanorod.
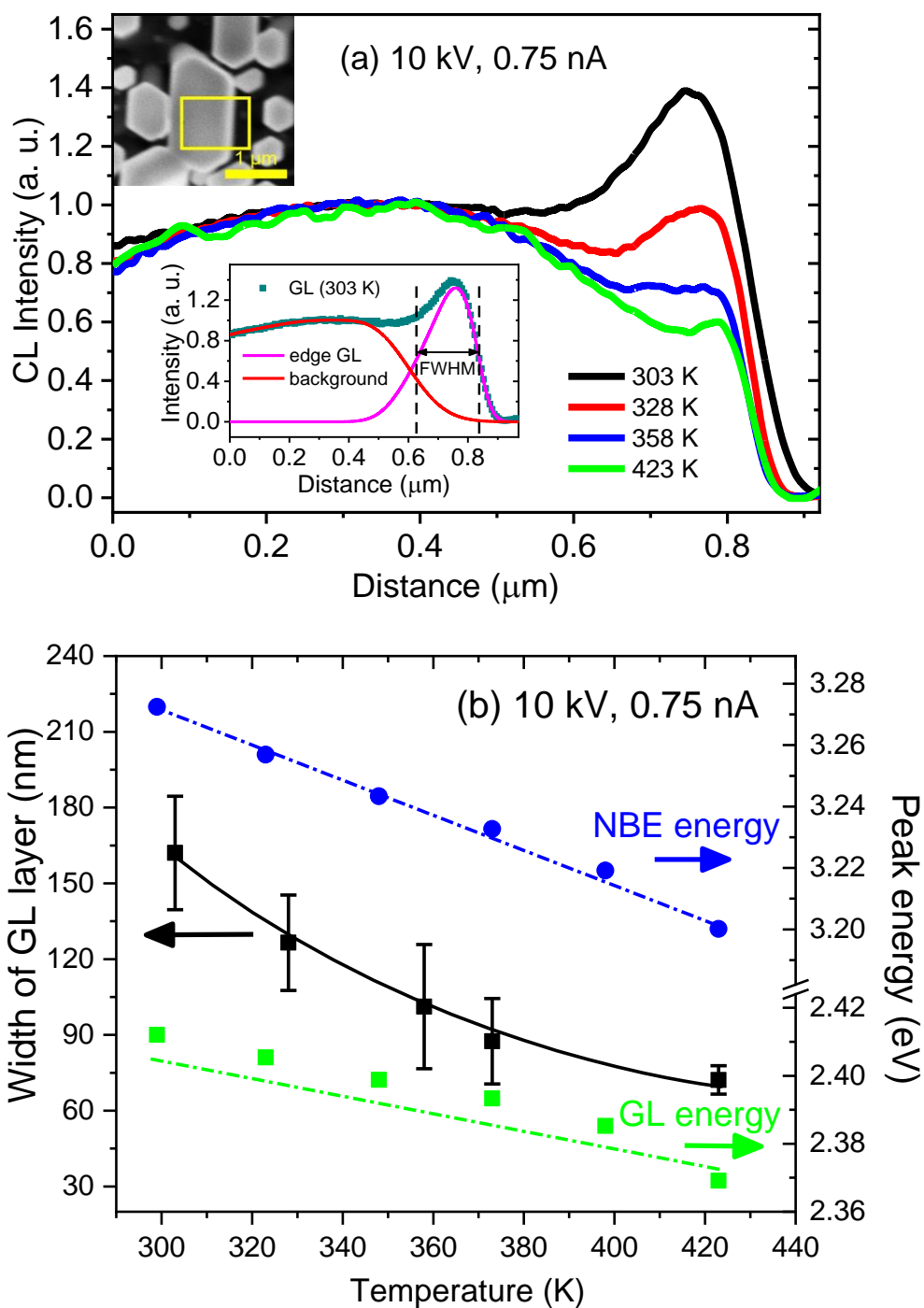
Figure 5. (a) Normalized line profiles of the GL emission across a nanorod edge at various temperatures. The yellow rectangle in the CL image indicates the area from which the data were extracted. The right half of the line profile could be fitted with a Gaussian function (inset), enabling estimation of the FWHM of the GL surface layer. (b) Variation of the FWHM of the GL layer as a fucntion of temperature, together with the GL and NBE peak energies.
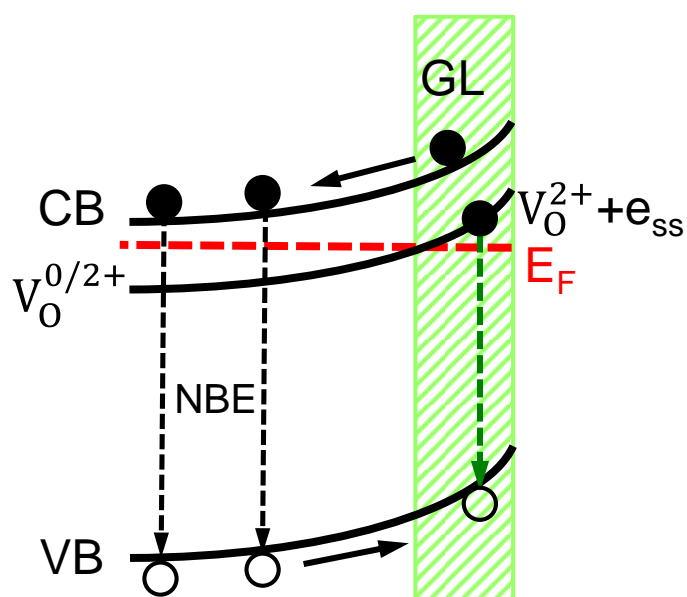
Figure 6. Schematic of the energy band diagram showing the band bending in the near-surface region of the $V_O^{0/2+}$ charge transfer level above the E_F converting V_O^0 to V_O^{2+} center which traps an electron from surface states to produce V_O^+. The vertical dotted lines depict the GL and NBE recombination channels. Electrons and holes in the band bending region are swept in opposite directions as depicted by the arrows in the conduction and valence bands.